

para-Phenylene-Bridged Spirobi(triarylamine) Dimer with Four Perpendicularly Linked Redox-Active π Systems

Akihiro Ito,^{*,[a]} Kazuhira Hata,^[a] Kensuke Kawamoto,^[a] Yasukazu Hirao,^[a, e] Kazuyoshi Tanaka,^[a] Motoo Shiro,^[b] Ko Furukawa,^[c] and Tatsuhisa Kato^[d]

Abstract: *para*-Phenylene-bridged spirobi(triarylamine) dimer **2**, in which π conjugation through four redox-active triarylamine subunits is partially segregated by the unique perpendicular conformation, was prepared and characterized by structural, electrochemical, and spectroscopic methods. Quantum chemical calculations (DFT and CASSCF) predicted that the frontier molecular orbitals of **2** are virtually fourfold degenerate, so that the oxidized states of **2** can give intriguing electronic and magnetic properties. In fact, the continuous-wave ESR spec-

troscopy of radical cation **2**^{•+} showed that the unpaired electron was trapped in the inner two redox-active dianisylamine subunits, and moreover was fully delocalized over them. Magnetic susceptibility measurements and pulsed ESR spectroscopy of the isolated salts of **2**, which can be prepared by treatment with SbCl₅, revealed that the generated tetracation **2**⁴⁺ decomposed

mainly into a mixture of 1) a decomposed tetra(radical cation) consisting of a tri(radical cation) moiety and a trianisylamine radical cation moiety ($\approx 75\%$) and 2) a diamagnetic quinoid dication in a tetraanisyl-*p*-phenylenediamine moiety and two trianisylamine radical cation moieties ($\approx 25\%$). Furthermore, the spin-quartet state of the tri(radical cation) moiety in the decomposed tetra(radical cation) was found to be in the ground state lying 30 cal mol⁻¹ below the competing spin-doublet state.

Keywords: arylamines • intervalent compounds • organic radicals • radical ions • spiro compounds

Introduction

Molecule-based electronics have recently attracted much interest with regard to breakthrough of the limit of silicon-based semiconductor technology.^[1–3] The development of integrated molecular-scale devices in the scope of nanotechnology necessarily requires the novel design and preparation of organic molecular components with predictable and controllable electrical, optical, and magnetic properties. In particular, characterization of the molecular and electronic structures of organic (multi)radicals is of great importance for our current understanding of efficient intramolecular electron (or hole) transport and spin–spin interaction, which is indispensable for practical applications of this type of molecular system in the future.

In this context, spiro linkage of spin-containing and/or redox-active molecular subunits has repeatedly been revisited in the field of molecule-based materials science.^[4–15] As shown in Figure 1, the spiro compounds have a unique structure in which the same two π -electron systems are linked with a so-called spiro atom, and consequently these two π faces are possibly oriented at 90° to one another. Hence, when a radical center is introduced into each π -electron

[a] Dr. A. Ito, K. Hata, K. Kawamoto, Dr. Y. Hirao, Prof. Dr. K. Tanaka
Department of Molecular Engineering
Graduate School of Engineering, Kyoto University
Nishikyo-ku, Kyoto 615-8510 (Japan)
Fax: (+81)75-383-2556
E-mail: aito@scl.kyoto-u.ac.jp

[b] Dr. M. Shiro
X-ray Research Laboratory, Rigaku Corporation
Matsubaracho 3-9-12, Akishima, Tokyo 196-8666 (Japan)

[c] Dr. K. Furukawa
Institute for Molecular Science
Myodaiji, Okazaki 444-8585 (Japan)

[d] Prof. Dr. T. Kato
Department of Chemistry, Josai University
1-1 Keyakidai, Sakado, Saitama 350-0295 (Japan)
Present address:
Institute for the Promotion of Excellence in Higher Education
Kyoto University
Yoshida-Nihonmatsu, Sakyo-ku, Kyoto 606-8501 (Japan)

[e] Dr. Y. Hirao
Present address: Department of Chemistry
Graduate School of Science
Osaka University, 1-1 Machikaneyamacho
Toyonaka, Osaka 560-0043 (Japan)

Supporting information for this article is available on the WWW under <http://dx.doi.org/10.1002/chem.201000848>.

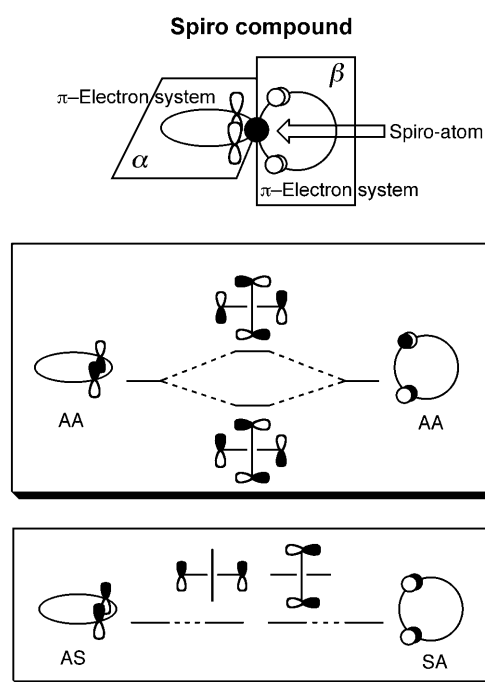


Figure 1. Schematic drawings of a spiro compound and two types of molecular orbital (MO) interactions between the same two π subunits that reside on the perpendicular molecular planes α and β , respectively, in the spiro structure. A and S denote antisymmetric and symmetric, respectively, with regard to the symmetry planes α and β .

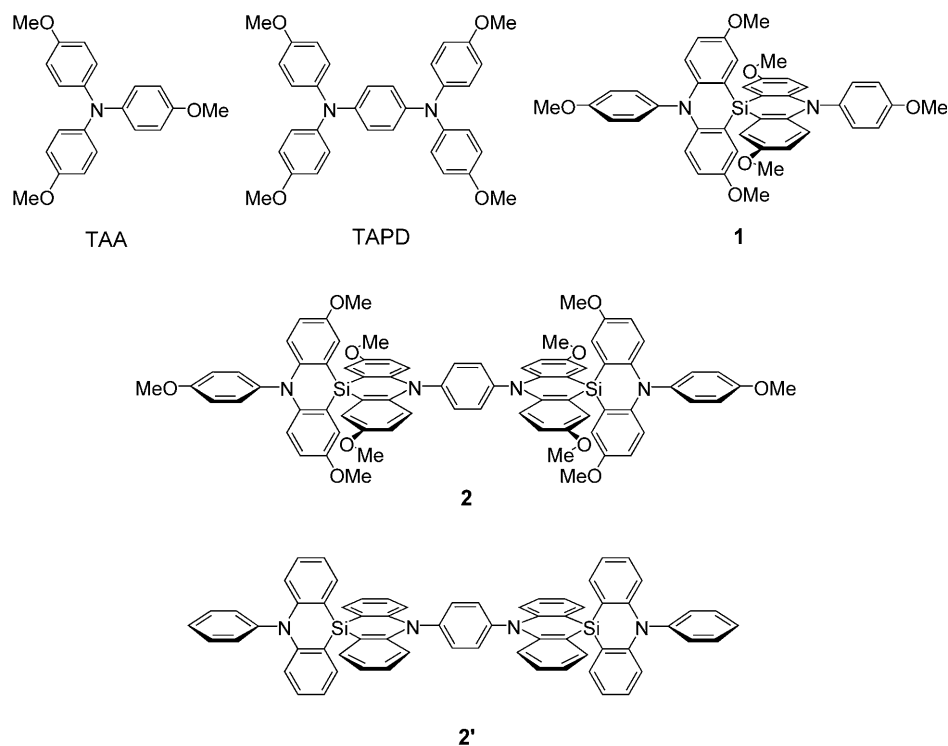
system, the orbital interaction between the same two singly occupied (SO) fragment molecular orbitals (MOs) of the mutually perpendicular π -electron systems can vary significantly depending on their symmetries (Figure 1).^[16] When both fragment MOs are antisymmetric to only one of the two symmetry planes (AS and SA), the orbital degeneracy gives rise to a parallel spin alignment between two unpaired electrons; when both fragment MOs are antisymmetric to both symmetry planes (AA), so-called spiro conjugation lifts the orbital degeneracy and thus leads to an antiparallel spin alignment between two unpaired electrons. With regard to the spin preference in spirobiradicals, Dougherty and co-workers examined the possibility of generating 1,4,6,9-spiro-[4,4]nonatetrayl from both theoretical and experimental points of view,^[4,5] and Kahn and co-workers reported the synthesis of a spiro-fused bis(nitronyl nitroxide) and the weak intramolecular antiferromagnetic interaction ($J_{\text{intra}}/k_{\text{B}} = -5.8$ K) between the two radical centers, which is probably due to the spiro conjugation.^[14] Recently, Ishida et al. revealed the presence of intermolecular antiferromagnetic interaction ($J_{\text{inter}}/k_{\text{B}} = -70$ K) in a spiro-fused bis(nitroxide) and estimated the intramolecular ferromagnetic interaction ($J_{\text{intra}}/k_{\text{B}} = 12\text{--}13$ K), which was probably buried by the large intermolecular antiferromagnetic interaction, on the basis of DFT calculations.^[15]

From the structural viewpoint, the geometrical orthogonality could obviate the possibility that the component molecules form a simple one-dimensional π -stacked crystal struc-

ture, which is often haunted with a diamagnetic property. For instance, the attempts aimed at constructing metallic charge-transfer salts with unique three-dimensional structures and molecular metals composed of a single molecular component were undertaken by using spiro molecules.^[7–12] In particular, Haddon and co-workers revealed that phenarenyl-based spiro molecules gave intriguing magnetic, electrical, and optical properties in the solid state, by taking advantage of the spiro conjugation and the nonplanar geometry of the multicentered radicals.^[9–12]

Recently, we reported the synthesis of the spiro-fused bis(triarylamine) **1** and the electronic structures of the cation $\mathbf{1}^+$ and dication $\mathbf{1}^{2+}$.^[17,18] The spiro molecule **1** has a unique structure in which two redox-active triarylamine (TAA) subunits are linked perpendicularly to one another through a spiro Si atom. Note that the choice of a Si linkage stems from the facile synthesis of the spiro structure, as described later. Gleiter and Böhm pointed out the possibility that the participation of 3d orbitals of the Si atom causes a considerable increase of spiro conjugation.^[19] However, quantum chemical calculations predicted that the degeneracy of magnetic orbitals (fragment SOMOs originating from the two TAA subunits) could be maintained for the dication $\mathbf{1}^{2+}$, and the two unpaired electrons could be ferromagnetically coupled.^[17] In fact, $\mathbf{1}^{2+}(\text{SbCl}_6^-)_2$ was a persistent diradical with a spin triplet multiplicity ($J_{\text{intra}}/k_{\text{B}} = 16$ K).^[17] On the other hand, we found that the radical cation $\mathbf{1}^+$ was characterized as an intriguing bis(triarylamine)-based intervalence charge-transfer (IVCT) molecule, and the thermal intramolecular spin-transfer (IST) rates were unequivocally determined by using variable-temperature electron spin resonance (VT-ESR) spectroscopy.^[18] The spiro structure and its suitability for molecular electronics have already been discussed from both theoretical^[6] and experimental^[7] viewpoints. The versatility of **1** is ascribed to 1) the capability of the stepwise formation of relatively stable radical cations originating from the multiredox properties of arylamine-based molecular systems and 2) the segmentation of the π -conjugated system due to the perpendicular molecular structure. With this point in mind, it is of great interest to extend **1** to oligomeric systems.

Herein, we report the synthesis, molecular structure, and electronic structure of *para*-phenylene-bridged spirobi(triarylamine) dimer **2**. The central part of **2** can be regarded as tetraanisyl-*para*-phenylenediamine (TAPD). However, the planar structure of the inner two dianisylamine (DAA) subunits unavoidably leads to the perpendicular conformation of the central TAPD moiety in **2**. In such a conformation, the dication of TAPD can no longer adopt the diamagnetic quinoid structure, and therefore the diradical character emerges from breaking of π conjugation between the inner two DAA subunits through *para*-phenylene. The *para*-phenylene-bridged di(radical cation)s have already been reported in comparison with their *meta*-phenylene-bridged counterpart.^[20–22] The present spirobi(triarylamine) dimer **2** is anticipated to realize the almost orthogonal configuration of the individual triarylamine-based π systems. Similar molecular



Results and Discussion

Theoretical considerations: To address the electronic structures of *para*-phenylene-bridged spiro(triarylamine) dimer **2**, we carried out DFT calculations (at the B3LYP/6-31G** level) on **2'**, the fully unsubstituted analogue of **2**.^[26] The optimized structure of **2'** was found to take the expected alternant perpendicular conformation with D_{2h} symmetry. The distance between the outer two N nuclei was calculated to be 18.581 Å, that between the inner two N nuclei, 5.682 Å, and that between the two N nuclei through the spiro Si atom, 6.449 Å. As shown in Figure 2, we found that the frontier MOs from HOMO to (HO-3)MO were virtually degenerate localized MOs. Moreover, the HOMO and (HO-1)MO were distributed mainly over the outer two

systems were previously examined by using anionic derivatives of oligo(9,10-anthrylene).^[23–25]

triarylamine subunits, whereas (HO-2)MO and (HO-3)MO were mainly over the inner two triarylamine subunits, and the two groups of MOs were separated by 0.07 eV. From this frontier MO structure, it is possible that the removal of

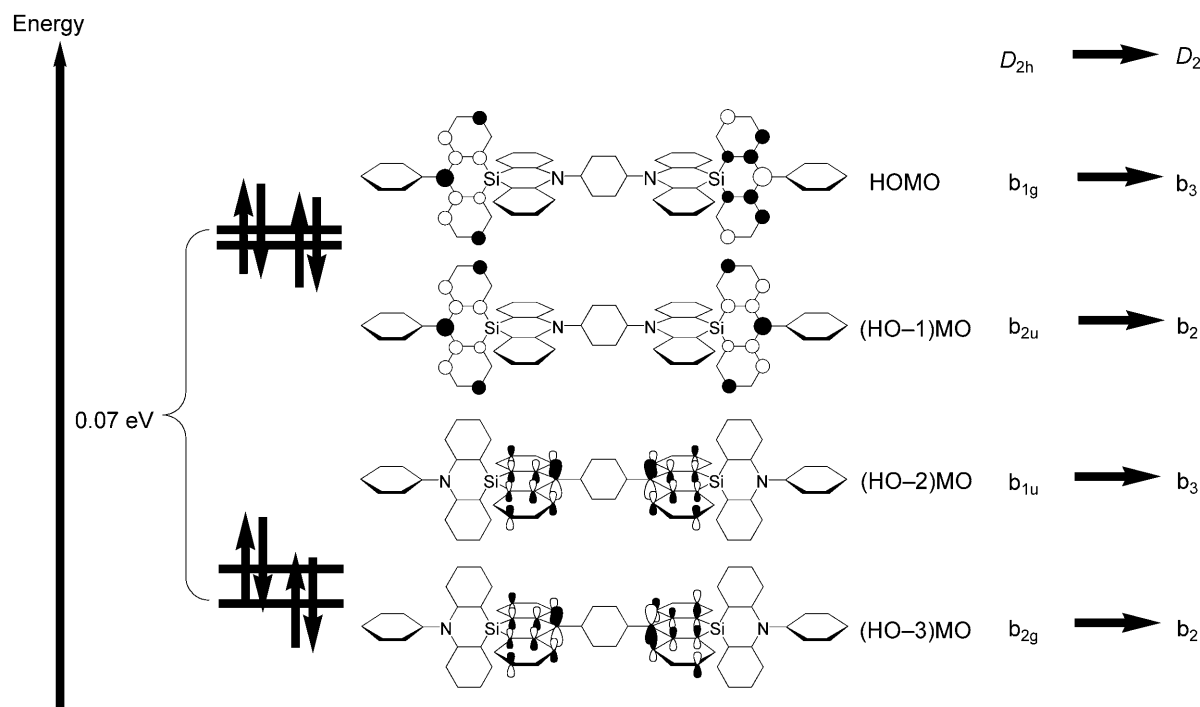


Figure 2. Frontier MOs for **2'** (B3LYP/6-31G**). These MOs are selected as the active space MOs in CAS(4,4)/3-21G calculations for **2⁴⁺**.

an electron causes the IST among the four triarylamine redox-active subunits, and furthermore, as is evident from the quasi-fourfold-degenerate MOs, the spin-quintet state can be fulfilled in tetracation 2^{4+} .

To predict the spin multiplicity for the highest oxidation state of **2**, we performed complete active space self-consistent field (CASSCF) calculations^[27] with the 3-21G basis set for the tetracation 2^{4+} , in which all the triarylamine subunits are being oxidized, and hence the competing spin states (singlet, triplet, and quintet states) should be considered.^[26] The active space orbitals adopted here were $54b_2$, $59b_3$, $55b_2$, and $60b_3$: we took account of all the configurations that arise when four electrons are allowed to occupy four MOs as shown in Figure 2. Note that the geometry optimization by the CAS(4,4) method resulted in the lowering of symmetry from D_{2h} to D_2 , and therefore the symmetry terms for the corresponding MOs were altered as shown in Figure 2.

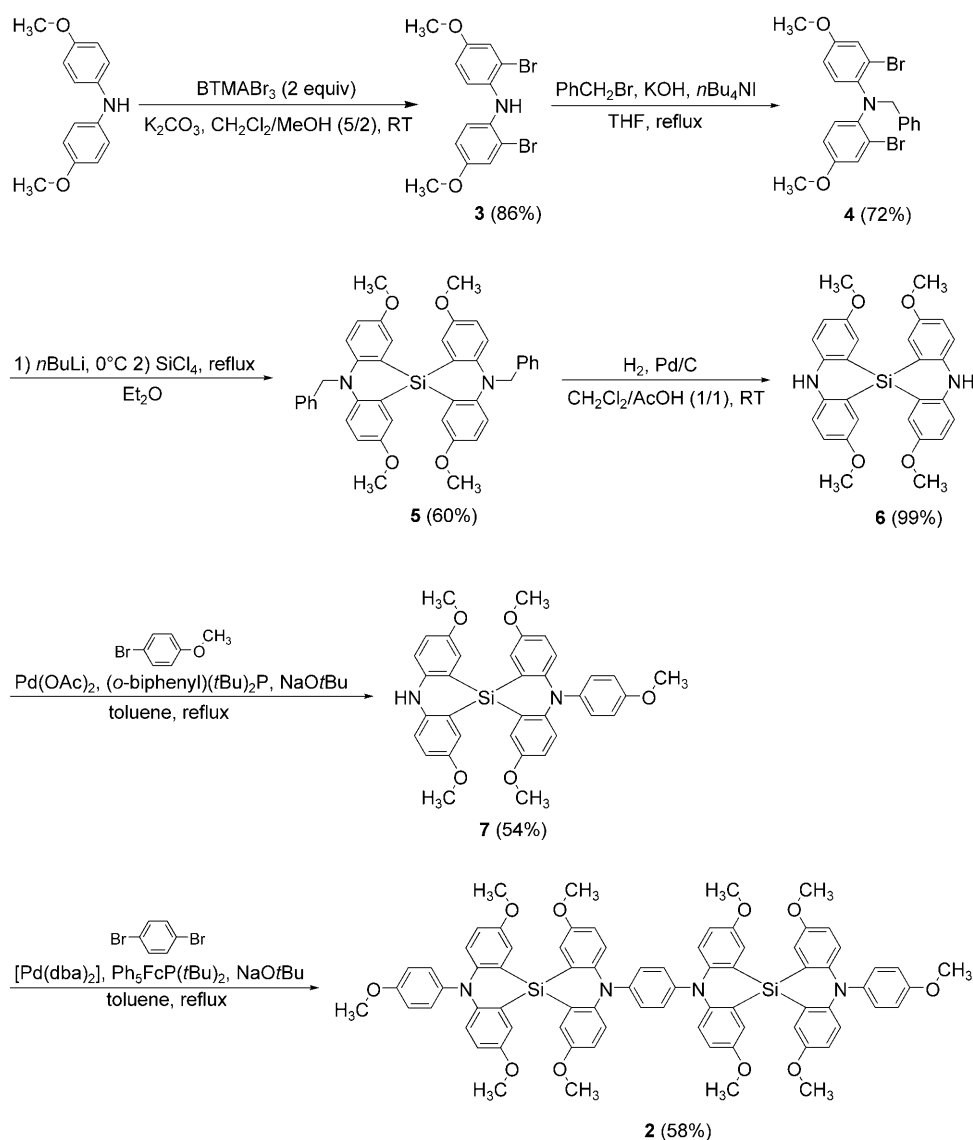
Table 1 lists the relative energies of three low-lying spin states. Although the ground state of the tetracation 2^{4+} was predicted to be the quintet 5A state, this result suggests that these three spin states were virtually degenerate at this level of theory. The fractional occupation numbers of all the spin states, 5A , 3B_1 , and 1A , were calculated to be 1.00, 1.00, 1.00, and 1.00, respectively, for the four active space orbitals, $54b_2$, $59b_3$, $55b_2$, and $60b_3$. This indicates that the tetracation 2^{4+} has a tetraradical character, which reflects the segregation of π conjugation due to the perpendicular molecular structure of **2'**. Again, it should be noted that the entire optimized molecular structures for the three spin electronic states of the tetracation 2^{4+} remained virtually unchanged, probably due to the perpendicular structure.

Synthesis and structural studies: para-Phenylene-bridged spirobi(triarylamine) dimer **2** was synthesized by following the procedure shown in Scheme 1. The synthesis of spiro structures often requires complicated synthetic routes. As a facile method to a spiro structure, we noted that Gilman and co-workers realized reasonable yields of spirobi(dihydrophena-

Table 1. Relative energies [cal mol⁻¹] of three low-lying states and configuration interaction (CI) coefficients of dominant configurations for the unsubstituted model compounds for **2** at the CAS(4,4)/3-21G*/CAS(4,4)/3-21G* level of theory.

State	Relative energy ^[a]	Configuration	Coefficient
5A	0.0	$(54b_2)^1(59b_3)^1(55b_2)^1(60b_3)^1$	1.00
1A	1.4	$(54b_2)^2(59b_3)^2$	-0.44
		$(54b_2)^2(55b_2)^2$	0.44
		$(55b_2)^2(60b_3)^2$	-0.43
3B_1	6.8	$(59b_3)^2(60b_3)^2$	0.43
		$(54b_2)^2(59b_3)^1(55b_2)^1$	0.50
		$(59b_3)^1(55b_2)^1(60b_3)^2$	-0.49
		$(54b_2)^1(59b_3)^2(60b_3)^1$	-0.51
		$(54b_2)^1(55b_2)^2(60b_3)^1$	0.51

[a] Energy relative to the optimized D_2 quintet state, for which a positive value indicates that the state lies above the 5A state; -3302.4767 hartree.



Scheme 1. Synthetic route for **2**. BTMABr₃ = benzyltrimethylammonium bromide, [Pd(dba)₂] = bis(dibenzylideneacetone)palladium.

zasiline)s by treatment of the corresponding *N*-alkyl-2,2'-dilithiodiphenylamine with silicon tetrachloride.^[28] By employing Gilman's method as a key reaction, the core compound, spiro-fused diamine **6**, was obtained in four steps starting from di(*p*-anisyl)amine.

One of the two amino groups of **6** was capped by a *p*-anisyl group with use of a Pd-catalyzed amination reaction (Buchwald–Hartwig reaction).^[29–32] Finally, the target molecule **2** was formed by the reaction of *p*-dibromobenzene with *p*-anisyl-capped spiro-fused diamine **7** by utilizing the same Pd-catalyzed amination reaction. Note that the use of the pentaphenylferrocenyl di-*tert*-butylphosphine ligand^[33,34] instead of the *o*-biphenyl di-*tert*-butylphosphine ligand,^[35] which was enough for the preparation of **7**, was essential for the preparation of the final coupling product **2**.

Colorless platelike single crystals were grown by slow evaporation of a dilute mixed solution (CH₃CN and CH₂Cl₂) of **2**, and its molecular structure was successfully established by means of X-ray structure analysis (Table 2 and Figure 3). The obtained crystals included four CH₃CN and one H₂O per molecule of **2**. As expected from the quantum chemical calculations as well as the molecular design in the Introduction, **2** adopted an alternately perpendicular structure, in which the amino planes linked by the spiro Si atom were perpendicularly placed and the central TAPD moiety also took a perpendicular conformation (the top and side views in Figure 3). The span of compound **2** was about 30 Å in length. The distance (N2–N2*) between the outer two N nuclei was calculated to be 18.349 Å, that (N1–N1*) between the inner two N nuclei, 5.647 Å, and that (N1–N2) between the two N nuclei through the spiro Si atom, 6.361 Å. Hence, the observed structural feature promises the predicted electronic structures of the oxidized species of **2**.

Electrochemical and spectroelectrochemical studies:

The redox behavior of *para*-phenylene-bridged spirobi(triarylamine) dimer **2**, in which four oxidizable subunits are connected by a spiro Si atom and *para*-phenylene, were investigated by cyclic voltammetry (CV) and differential pulse voltammetry (DPV) in CH₂Cl₂ at room temperature (Figure 4). The cyclic voltammogram of **2** showed three redox couples at +0.21,

Table 2. Crystallographic data for **2**·(CH₃CN)₄·(H₂O).

empirical formula	C ₈₄ H ₈₀ N ₈ O ₁₁ Si ₂
formula weight	1433.77
<i>T</i> [K]	93(1)
λ [Å]	1.54187
crystal system	triclinic
space group	<i>P</i> $\bar{1}$
<i>Z</i>	1
<i>a</i> [Å]	9.85268(18)
<i>b</i> [Å]	11.1752(2)
<i>c</i> [Å]	18.9661(7)
α [°]	75.4725(10)
β [°]	74.9816(10)
γ [°]	66.6937(9)
<i>V</i> [Å ³]	1826.28(8)
ρ_{calcd} [g cm ⁻³]	1.304
μ [mm ⁻¹]	10.017
collected data	20510
unique data/ <i>R</i> _{int}	6478/0.075
no. of parameters	486
goodness-of-fit ^[a]	0.971
<i>R</i> 1 (<i>I</i> > 2 σ), <i>wR</i> 2 (all reflections) ^[b]	0.0714, 0.2049
residual density [e Å ⁻³]	0.35/–0.40

[a] GOF = $\left\{ \frac{\sum [w(F_0^2 - F_c^2)]^2}{(n - p)} \right\}^{1/2}$, in which *n* and *p* denote the number of data and parameters. [b] *R*1 = $\frac{\sum (\|F_0\| - \|F_c\|)}{\sum \|F_0\|}$ and *wR*2 = $\left\{ \frac{\sum [w(F_0^2 - F_c^2)]^2}{\sum [w(F_0^2)]} \right\}^{1/2}$, in which $w = 1 / [\sigma^2(F_0^2) + (aP)^2 + bP]$ and $P = \frac{1}{3}[(\text{Max}_i F_i^2) + 2F_c^2]$.

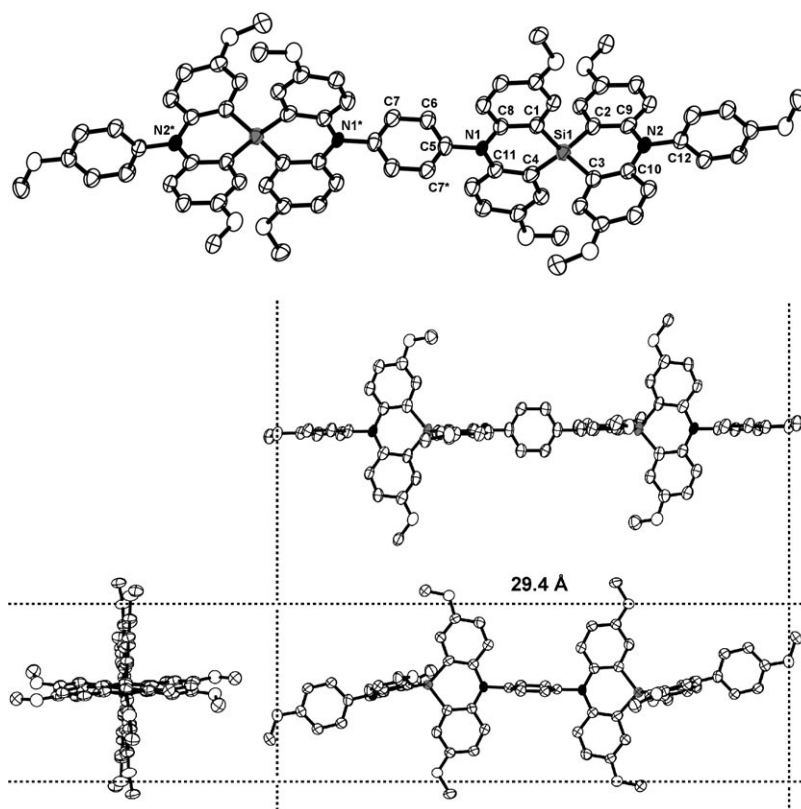


Figure 3. Molecular structure of **2** with atomic numbering scheme and the top and side views. Hydrogen atoms are omitted for clarity. Selected bond lengths [Å] and angles [°]: Si1–C1 1.841(3), Si1–C2 1.821(4), Si1–C3 1.847(4), Si1–C4 1.827(3), N1–C5 1.442(4), N1–C8 1.410(5), N1–C11 1.426(4), N2–C9 1.421(4), N2–C10 1.427(5), N2–C12 1.441(5), C5–C6 1.374(4), C6–C7 1.388(5); C1–Si1–C4 100.90(16), C2–Si1–C3 101.52(16), C8–N1–C11 126.6(2), C9–N2–C10 125.6(3), C6–C5–C7* 120.1(3), C5–C6–C7 120.0(3).

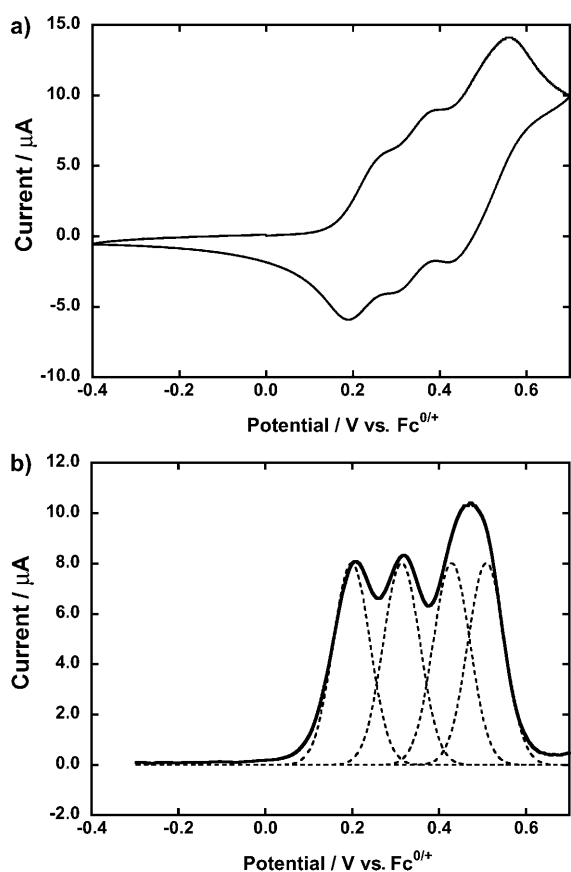
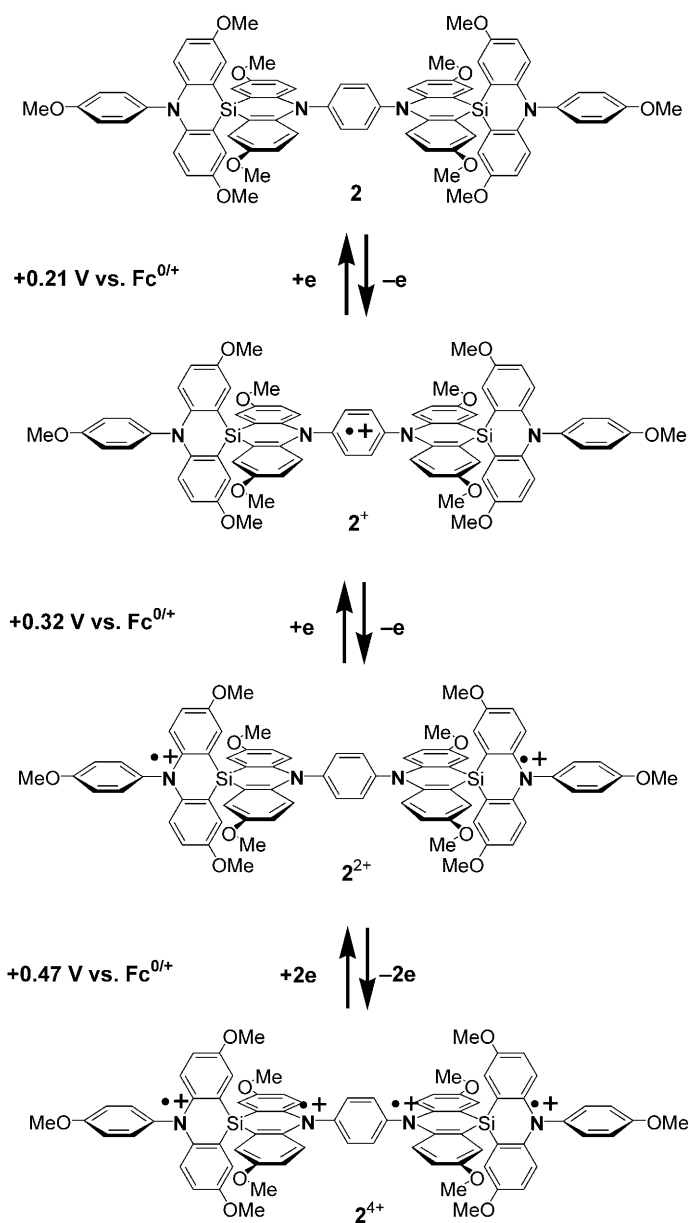


Figure 4. a) Cyclic voltammogram and b) differential pulse voltammogram of **2**, measured in CH_2Cl_2 containing $0.1\text{ M } n\text{Bu}_4\text{NBF}_4$ at 298 K (scan rate 100 mV s^{-1}).

$+0.32$, and $+0.47\text{ V}$ (vs. $\text{Fc}^{0/+}$) and the last oxidation process corresponds to quasi-two-electron transfer judging from the observed current ratio (Scheme 2). From the curve fitting of the observed differential pulse voltammogram, such a quasi-two-electron oxidation process was found to be separable into two reversible one-electron oxidation processes ($E_3 = +0.43$ and $E_4 = +0.51\text{ V}$ (vs. $\text{Fc}^{0/+}$); broken lines in Figure 4b). The oxidation potentials of **2** are summarized in Table 3 together with those of the related compounds under the same conditions. Note that the reported oxidation potentials for **1** were measured in MeCN .^[17,18] As is apparent from the recent cautionary reports, the oxidation potentials and their differences are influenced strongly by the solvent and the supporting electrolyte used in the CV measurements.^[36–39] Hence, we have remeasured the oxidation potentials for **1** in CH_2Cl_2 solution in this study.

First of all, the $E_2 - E_1 (= \Delta E)$ value for **2** decreases by half relative to that of **1**. This difference in ΔE between **1** and **2** originates from the fact that the first two successive one-electron oxidation processes in **2** take place from the two spiro-fused bis(trianisylamine) units, whereas those in **1** occur from the two TAA subunits within the spiro-fused bis(trianisylamine). However, the small, but not negligible, value of ΔE for **2** indicates that the radical cation **2⁺** is sta-



Scheme 2. Three-stage redox reaction sequence for **2**.

bilized by the spin delocalization between the two spiro-fused bis(trianisylamine) units through the central *para*-

Table 3. Oxidation potentials [V vs. $\text{Fc}^{0/+}$] for **1**, **2**, TAA, and TAPD.^[a]

Compound	E_1	E_2	E_3	E_4	$E_2 - E_1 (= \Delta E)$
1	0.26	0.46	–	–	0.20
	(0.31)	0.44	–	–	(0.13) ^[b]
2	0.21	0.32	–	0.47 ^[c]	0.11
	0.20 ^[d]	0.32 ^[d]	0.43 ^[d]	0.51 ^[d]	0.12
TAA	0.11				
TAPD	–0.10	0.36	–	–	0.46

[a] $1\text{ mM } \text{CH}_2\text{Cl}_2$ solution containing $0.1\text{ M } n\text{Bu}_4\text{NBF}_4$, Pt electrode, 100 mV s^{-1} , 298 K . [b] Measured in $1\text{ mM } \text{MeCN}$ solution. [c] Quasi-two-electron transfer. [d] Estimated from the Gaussian curve fitting of the measured differential pulse voltammogram.

phenylene bridging unit. The ΔE value (0.20 V) for **2** should rather be compared with the ΔE value (0.46 V) for TAPD, and the small ΔE value for **2** suggests that the perpendicular conformation of the central *para*-phenylene bridging unit makes it difficult to take the semi-quinoid structure, which is the origin of the stability of the TAPD radical cation.

More noteworthy is that the differences in E_1 and E_2 between **1** and **2** (the differences decrease by 0.05 and 0.14 V, respectively, on going from **1** to **2**) indicate that the stabilization of the radical cation and dication of **2** can be enhanced compared to those of **1**. As will be clarified from the ESR studies, the stabilization of the radical cation of **2** originates from the spin delocalization between the two spiro-fused bis(trianisylamine) units through the central *para*-phenylene bridging unit, whereas the stabilization of the dication of **2** probably stems from the change of the charge distribution from the inner two DAA subunits in 2^+ to the outer two TAA subunits in 2^{2+} .

To obtain more information about the unique electronic states for the oxidized species of **2**, we measured the optical absorption spectral changes of **2** in CH_2Cl_2 during the course of oxidation going from neutral **2** to tetracation 2^{4+} by using an optically transparent thin-layer electrochemical cell (Figure 5). Throughout the oxidation process of **2** to 2^{4+} ,

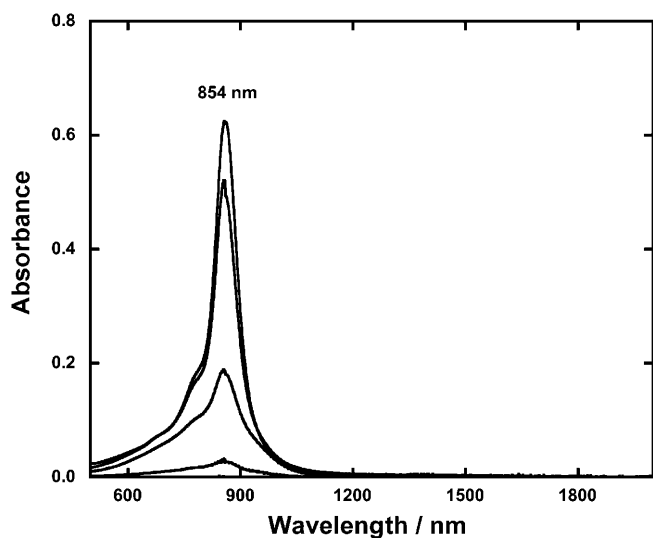


Figure 5. Vis-NIR spectral change during the electrochemical oxidation of **2** to 2^{4+} in $\text{CH}_2\text{Cl}_2/0.1\text{ M } n\text{Bu}_4\text{NBF}_4$ at 298 K.

an intense absorption band characteristic for radical cations of triarylamines appeared and grew monotonously at 854 nm, and no IVCT [or charge-resonance (CR)] band was observed in the near-infrared (NIR) region (up to 2000 nm). On the other hand, as will be clarified from the ESR studies, there is charge delocalization in 2^+ . To search for the CR band in the absorption spectrum of 2^+ , we investigated the solvent effect on the absorption spectrum of 2^+ . We chose *n*-butyronitrile and $\text{CH}_2\text{Cl}_2/\text{Et}_2\text{O}$ as higher-polarity ($\epsilon > 20$) and lower-polarity ($\epsilon < 10$) solvents, respectively. Unfortu-

nately, we could not find any indication of the appearance of a CR band for 2^+ (see Figure S1 in the Supporting Information for details).

The observed monotonous spectral changes of **2** are similar to those of **1**.^[18] This result suggests that the perpendicular molecular structure remains unchanged throughout the oxidation process of **2** to 2^{4+} , and suggests the independence of each triarylamine redox-active subunit from the other redox-active ones. On the other hand, the redox property of **2** demonstrated the electronic coupling (or π conjugation) among the four triarylamine-based π systems. The elucidation of this discrepancy probably needs more theoretical development.

Characterization of radical cation 2^+ : When **2** was treated with 0.8 equiv of tris(4-bromophenyl)aminium hexachloroantimonate ($\text{TBA}\cdot\text{SbCl}_6$)^[40] as oxidant at 195 K in *n*-butyronitrile/toluene (1:1, v/v), the generation of the corresponding radical cation was detected by the use of X-band ESR spectroscopy. At room temperature, the radical cation 2^+ afforded the ESR spectrum shown in Figure 6a. The observed spectrum is roughly explainable by a 1:2:3:2:1 intensity pattern owing to the hyperfine coupling of the unpaired electron with two out of the four equivalent ^{14}N ($I=1$) nuclei attributed to the four triarylamine redox-active subunits. Furthermore, the observed spectrum can be simulated equally by the assumption of complete delocalization between the inner two nitrogen centers. The observed ESR line shape can be well simulated in terms of the hyperfine interactions with one ^{14}N ($I=1$) nucleus ($a_{\text{N}}(2\text{N})=0.63\text{ mT}$), two *ortho* ^1H ($I=1/2$) nuclei ($a_{\text{H}(\text{ortho})}(4\text{H})=0.12\text{ mT}$), six ^1H ($I=1/2$)

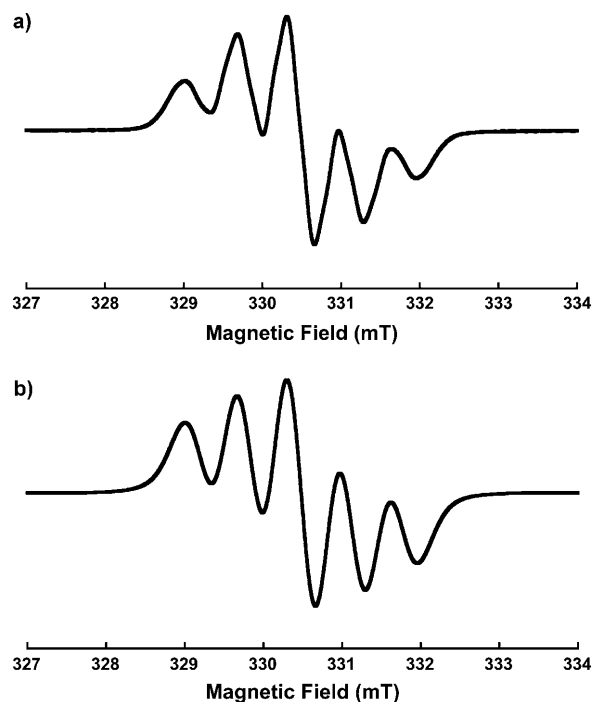


Figure 6. a) Continuous-wave (cw) ESR spectrum of 2^+ in CH_2Cl_2 at 293 K, and b) the simulated spectrum.

nuclei belonging to the *para*-substituted methoxy groups ($a_{\text{H(methoxy)}}(12\text{H})=0.08\text{ mT}$), and the incorporation of the contributions from the other nuclei into the constant line width of the spectral simulation (Figure 6b). More interestingly, the observed five-line ESR patterns remained almost unchanged over a relatively wide temperature range, as shown in Figure 7. The present observation indicates that the unpaired spin generated in 2^+ is confined in the inner two DAA subunits (or TAPD moiety), and moreover is fully delocalized over them.

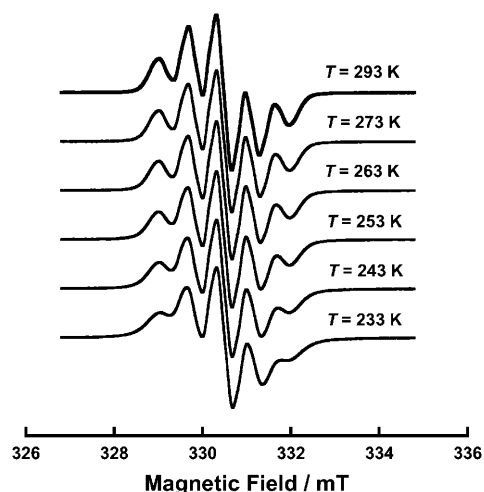


Figure 7. Temperature dependence of the cw-ESR spectrum for 2^+ in CH_2Cl_2 .

Characterization of dication 2^{2+} : Additional oxidation of 2^+ with $\text{TBA}\cdot\text{SbCl}_6$ at 195 K led to the generation of 2^{2+} . However, neither the definitive fine structure in the allowed resonance ($\Delta M_S = \pm 1$) nor the forbidden resonance ($\Delta M_S = \pm 2$) was detected in the cw-ESR spectrum in a rigid glass of *n*-butyronitrile at 123 K, whereas the ESR intensity of 2^{2+} increased up to nearly twice that of 2^+ (Figure S2 in the Supporting Information). In addition, the pulsed ESR measurements for 2^{2+} also confirmed the existence of the spin-doublet state of 2^{2+} at 5 K. These results strongly suggest that the two generated unpaired electrons are separately distributed over the outer two TAA subunits to avoid the unfavorable Coulombic repulsion between the charged centers, and therefore there is only a negligibly weak exchange interaction between the two unpaired spins.

Characterization of oxidized species of **2 generated by treatment with SbCl_5 :** Judging from the observed oxidation potentials, it is expected that **2** is fully oxidized into the tetracation 2^{4+} by using SbCl_5 as an oxidant. As shown in Figure 8a, the cw-ESR spectrum of the oxidized species of **2** treated with a 1 M CH_2Cl_2 solution of SbCl_5 at 195 K did not show a definite fine structure assignable to the spin-quintet state of 2^{4+} at 123 K, although the forbidden half-field transition was detected due to the existence of oxidized species with a spin multiplicity higher than $S=1$.^[41]

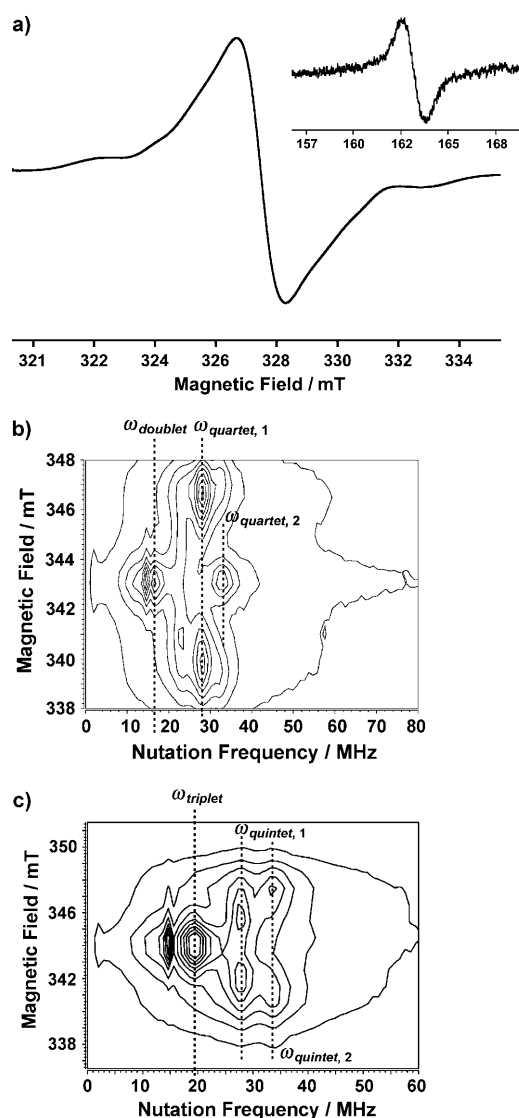


Figure 8. a) cw-ESR spectrum of the oxidized species of **2** treated by SbCl_5 in CH_2Cl_2 at 123 K. Inset: the forbidden half-field resonance at 123 K. b) 2D ESTN spectrum of the oxidized species of **2** treated by SbCl_5 in CH_2Cl_2 at 5 K. c) 2D ESTN spectrum of the as-oxidized species of **2** treated by SbCl_5 in CH_2Cl_2 at 5 K.

To identify the spin multiplicity of the fully oxidized species of **2** at low temperatures, we recorded the electron spin transient nutation (ESTN) spectrum based on the pulsed ESR method.^[42–45] As shown in Figure 8b, the 2D contour plot of the ESTN spectrum clearly displayed the intense nutation frequency peaks at $\omega_{\text{nutation}}=28$ and 32 MHz, as well as that corresponding to the doublet impurities ($\omega_{\text{doublet}}=16\text{ MHz}$). A frequency ratio of $\omega_{\text{nutation}}/\omega_{\text{doublet}}=28:16$ and $32:16$ demonstrated that the observed two frequencies are attributable to two kinds of transition for the spin-quartet state [$\omega_{\text{nutation}}/\omega_{\text{doublet}}=\sqrt{3}$ for the $|3/2, \pm 3/2\rangle \Leftrightarrow |3/2, \pm 1/2\rangle$; $\omega_{\text{nutation}}/\omega_{\text{doublet}}=2$ for the $|3/2, +1/2\rangle \Leftrightarrow |3/2, -1/2\rangle$]. Consequently, this observation established that the spin electronic state for the dominant species of **2** oxidized by SbCl_5 is in a spin-quartet state ($S=3/2$). However, this result indicated

that the observed spin electronic state did not agree with the spin-quintet state of 2^{4+} , which can be expected to be generated by using SbCl_5 as oxidant.

In the sample preparation for the above-mentioned ESR measurements, the oxidized solution was bubbled through Ar gas for about 30 s at 195 K in order to stir it. On the other hand, when the oxidized solution was kept in liquid nitrogen immediately after addition of SbCl_5 , the situation changed completely. As shown in Figure 8c, the 2D contour plot of the ESTN spectrum clearly showed the nutation frequency peaks at $\omega_{\text{nutation}} = 27.5$ and 33.8 MHz, as well as that corresponding to the competing triplet state (19.5 MHz). A frequency ratio of $\omega_{\text{nutation}}/\omega_{\text{triplet}}$ demonstrated that the observed two frequencies are attributable to two kinds of transition for the spin-quintet state of 2^{4+} [$\omega_{\text{nutation}}/\omega_{\text{doublet}} = 2/\sqrt{2}$ for the $|2, \pm 2\rangle \Leftrightarrow |2, \pm 1\rangle$; $\omega_{\text{nutation}}/\omega_{\text{doublet}} = \sqrt{6}/\sqrt{2}$ for the $|2, \pm 1\rangle \Leftrightarrow |2, 0\rangle$]. This observation suggests that the generated tetracation 2^{4+} is highly unstable at elevated temperatures, and therefore it is expected that the immediate decomposition of 2^{4+} into the spin-quartet and doublet species takes place through C–Si bond cleavage, which was already reported for 1^{+} in solution at room temperature.^[18]

Fortunately, we were able to isolate the oxidized species of **2** as the SbCl_6^- salt by adding dry ether to a CH_2Cl_2 solution of **2** oxidized with a 1 M CH_2Cl_2 solution of SbCl_5 at 195 K. The elemental analysis of the isolated powder exhibited a reasonable result close to $2^{4+}(\text{SbCl}_6^-)_4$, and at least indicated that all the triarylamine units in **2** were fully oxidized.^[46] To confirm the spin state of the isolated salt, the magnetic susceptibility of the powder sample of the isolated salt was measured on a superconducting quantum interference device (SQUID) magnetometer in the temperature range 2–300 K at a constant magnetic field of 500 G. The temperature dependence of the molar magnetic susceptibility (χ_M) is shown in Figure 9.

To elucidate the magnetic properties of the isolated salt, we assumed that the generated tetracation was readily decomposed by two kinds of C–Si bond cleavage processes:

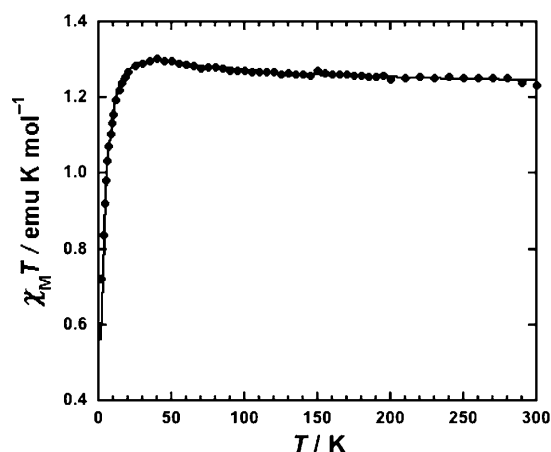


Figure 9. Temperature dependence of $\chi_M T$ for the isolated salts of **2** under a magnetic field of 500 G. The solid line represents the best fit to Equation (2).

1) one of the two spiro structures is decomposed to yield a tri(radical cation) moiety and a TAA radical cation moiety (route 1); 2) all the spiro structures are decomposed to yield a diamagnetic quinoid dication in the TAPD moiety and two TAA radical cation moieties (route 2), as shown in Scheme 3. Such a C–Si bond cleavage process has already been observed for 1^{+} in solution at room temperature.^[18] It should be noted that, in ref. [18] and this study, it has not been clarified how the vacant valencies after cleavage of the C–Si bonds are saturated. Judging from the elemental analysis of the isolated decomposed salt, however, the vacant valencies are probably compensated by the extraction of the hydrogen atoms from solvent molecules and/or the trace of water in the solution. Taking the above-mentioned assumption into consideration, we carried out the fitting of the temperature dependence of the magnetic susceptibility observed for the isolated salt. As shown in Figure 10, the interacting three-spin system for the tri(radical cation) moiety can be represented by a triangular scheme, in which each side of the triangle stands for the strength of the exchange coupling parameters J_{ij} between two spin centers S_i and S_j . In this case, the spin Hamiltonian can be written as Equation (1):

$$H = -2(J_{12}S_1S_2 + J_{23}S_2S_3 + J_{31}S_3S_1) \quad (1)$$

For the putative molecular structure for the tri(radical cation) moiety in the decomposed tetra(radical cation) shown by route 1 in Scheme 3, we adopted a general triangular scheme ($J_{12} \neq J_{23} \neq J_{31}$).^[47] As a whole, we used the formula expressed by Equation (2), in which the energy differences between three spin states Δ_1 and Δ_2 (Figure 10) are defined by Equations (3) and (4):

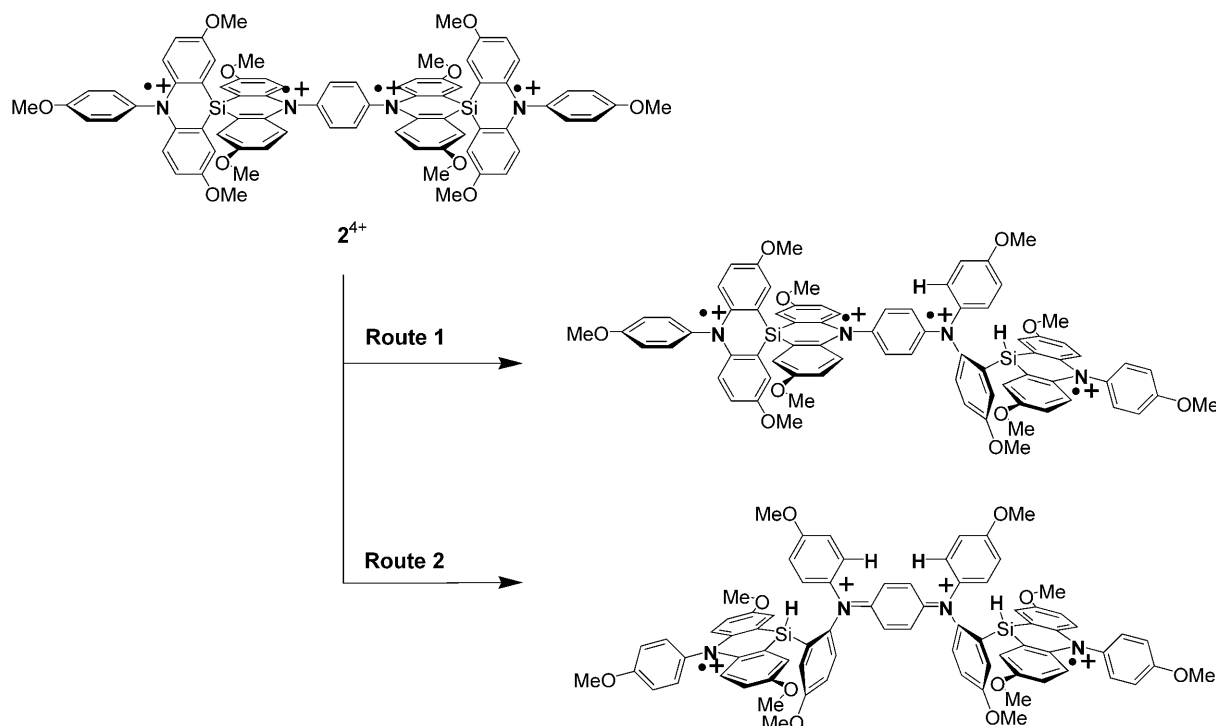
$$\chi_M T = f \frac{N_A g^2 \mu_B^2}{4k_B} \left[a \frac{1 + \exp(-\frac{\Delta_1}{k_B T}) + 10 \exp(-\frac{\Delta_2}{k_B T})}{1 + \exp(-\frac{\Delta_1}{k_B T}) + 2 \exp(-\frac{\Delta_2}{k_B T})} \frac{T}{T - \theta} + (2 - a) \frac{T}{T - \theta} \right] \quad (2)$$

$$\Delta_1 = 2\sqrt{J_{12}^2 + J_{23}^2 + J_{31}^2 - J_{12}J_{23} - J_{23}J_{31} - J_{31}J_{12}} \quad (3)$$

$$\Delta_2 = \frac{\Delta_1}{2} - (J_{12}J_{23}J_{31}) \quad (4)$$

Here we assume that the intermolecular magnetic interaction can be treated with mean field theory (the Curie–Weiss law). The purity factor f represents the purity of the salt including all the other experimental errors, and parameter a stands for the ratio in which only one of the two spiro structures is decomposed (route 1 in Scheme 3). Thus, the second term on the right-hand side of Equation (2) represents the Curie–Weiss behavior due to spin-1/2 of the TAA radical cations. The other constants, N_A , g , k_B , μ_B , and θ are the Avogadro number, the g -factor, the Boltzmann constant, the Bohr magneton, and the Weiss constant, respectively.

Although Equations (2)–(4) contain too many parameters to determine the three exchange coupling parameters J_{ij}



Scheme 3. Plausible routes toward the decomposition of tetracation 2^{4+} .

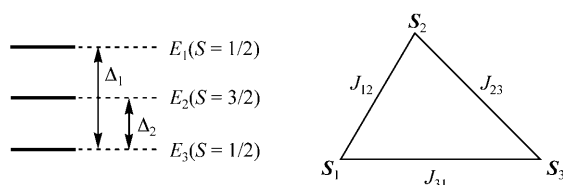


Figure 10. Energy level diagram for the two spin-doublet states and the one spin-quartet state originating from the magnetic interaction of a three-spin system, $S_1=S_2=S_3=1/2$.

uniquely, we can determine at least the energy differences among the competing three spin states, Δ_1 and Δ_2 , by the least-squares fitting of the experimental data to Equation (2) as a function of Δ_1 and Δ_2 . As a result, the best-fitted parameters were determined: $f=0.95$, $a=0.72$, $\Delta_1/k_B=54.3$ K, $\Delta_2/k_B=-15.2$ K, $\theta=-4.2$ K. The negative value of Δ_2 indicates that the spin-quartet state is the ground state of the tri(radical cation) moiety in the decomposed tetra(radical cation) (Scheme 3, route 1), and that the energy difference between the quartet and the low-lying doublet state is 30.2 cal mol $^{-1}$. From the simulated value for a , the dominant oxidized species of the isolated salt was estimated to be the decomposed tetra(radical cation) containing the tri(radical cation) moiety with spin-quartet ground state. The reproducibility of this result was confirmed by several trials. Finally, these analyses of the observed magnetic behavior for the isolated salts were consistent with those obtained by the pulsed ESR studies.

Conclusion

Electronic structures for the oxidized species of *para*-phenylene-bridged spirobi(triarylamine) **2** possessing perpendicular redox-active π systems were studied by using cw-ESR and pulsed ESR spectroscopy, and SQUID magnetometry. It was found that the unpaired electron in 2^{2+} was trapped in the inner two redox-active dianisylamine subunits (or TAPD moiety), and moreover was fully delocalized over them. On the other hand, 2^{4+} , the highest oxidation state of **2**, was found to be readily decomposed into the diamagnetic, spin-quartet, and spin-doublet species probably due to a weakness of the C–Si bond, judging from the temperature dependence of the magnetic susceptibility. However, it was clearly demonstrated that the ferromagnetic interaction among three spins-1/2 prevails in the tri(radical cation) moiety in the decomposed tetra(radical cation). Hence, the efforts toward the extended high-spin molecular systems utilizing **2** should still not be discarded. For instance, substitution of the other atoms for the present spiro Si atom may obviate the decomposition that we encountered in the present study.

Experimental Section

General information: Toluene and *n*-butyronitrile were distilled from CaH $_2$ under an argon atmosphere, tetrahydrofuran (THF) was distilled from sodium-benzophenone or potassium-benzophenone under an argon atmosphere, *N,N*-dimethylformamide (DMF) was dried over 4 Å molecu-

lar sieves, and benzonitrile was purified through an alumina (ICN, Alumina N, Akt. I) column with bubbling of argon, just before use. All the other purchased reagents and solvents were used without further purification. Column chromatography was performed with silica gel (Kanto Chemical Co., Inc., silica gel 60N, spherical neutral) or alumina (Kanto Chemical Co., Inc., aluminum oxide activated for column chromatography).

¹H and ¹³C spectra were recorded on a JEOL JNM-AL400 FT NMR spectrometer and chemical shifts are given in parts per million (ppm) relative to internal tetramethylsilane ($\delta=0.00$ ppm). Elemental analyses were performed by the Center for Organic Elemental Microanalysis, Kyoto University.

CV measurements were carried out in CH₂Cl₂ solution containing *n*-tetrabutylammonium tetrafluoroborate (TBABF₄, 0.1 M) as a supporting electrolyte (298 K, scan rate 100 mV⁻¹) with an ALS/chi Electrochemical Analyzer Model 612A. A three-electrode assembly was used, which was equipped with a platinum disk (2 mm²), a platinum wire, and Ag/0.01 M AgNO₃ (acetonitrile) as the working, counter, and reference electrodes, respectively. The observed redox potentials were referenced against the ferrocene/ferrocenium (Fc/Fc⁺) couple in CH₂Cl₂ solution.

UV/Vis-NIR spectra were obtained with a Perkin-Elmer Lambda 19 spectrometer. Spectroelectrochemical measurements were carried out with a custom-made optically transparent thin-layer electrochemical (OTTLE) cell (light pass length=1 mm) equipped with a platinum mesh, a platinum coil, and a silver wire as the working, counter, and pseudo-reference electrodes, respectively. The potential was applied with an ALS/chi Electrochemical Analyzer Model 612A.

ESR spectra were recorded on a JEOL JES-SRE2X X-band ESR spectrometer, in which temperature was controlled by a JEOL DVT2 variable-temperature unit. A Mn²⁺/MnO solid solution was used as a reference for the determination of *g*-values and hyperfine coupling constants. Pulsed ESR measurements were carried out on a Bruker ELEXSYS E580 X-band FT ESR spectrometer, in which temperature was controlled by an Oxford ITC503 temperature controller combined with an ESR 910 continuous-flow cryostat.

Magnetic susceptibilities of the powder samples were measured by a Quantum Design MPMS-5S system. The raw data were corrected for both the magnetization of sample holder alone and the diamagnetic contribution of the sample itself. The estimation of the diamagnetic contribution was done by using Pascal's constants.

2,2'-Dibromo-4,4'-dimethoxydiphenylamine (3): BTMABr₃ (34.9 g, 89.0 mmol) was added in one portion to a stirred suspension of dianisylamine (10.0 g, 43.6 mmol) and K₂CO₃ (18.1 g, 130 mmol) in a mixed solvent of CH₂Cl₂ (400 mL) and CH₃OH (160 mL), and the reaction mixture was stirred overnight. The solvent was removed in vacuo. After addition of water and CH₂Cl₂, the organic layer was separated and dried over Na₂SO₄. After evaporation of the solvent, the crude product was purified by column chromatography on silica gel (CH₂Cl₂/*n*-hexane=1:1 as eluent) and was recrystallized from *n*-hexane to afford **3** as a white crystalline solid (14.5 g, 86.9%). ¹H NMR (400 MHz, CDCl₃): $\delta=7.13$ (d, ⁴*J*=3.0 Hz, 2H; H-3), 7.13 (d, ³*J*=9.0 Hz, 2H; H-6), 6.77 (dd, ³*J*=9.0, ⁴*J*=3.0 Hz, 2H; H-5), 5.81 (br-s, 1H; NH), 3.76 ppm (s, 6H; OCH₃); ¹³C NMR (100 MHz, CDCl₃): $\delta=154.6$ (C-4), 134.8 (C-1), 119.7 (C-2 or C-6), 118.1 (C-2 or C-6), 115.0 (C-3), 114.3 (C-5), 55.8 ppm (OCH₃); elemental analysis calcd (%) for C₁₄H₁₃Br₂NO₂: C 43.44, H 3.39, Br 41.28, N 3.62; found: C 43.18, H 3.28, Br 41.39, N 3.50.

***N*-Benzyl-2,2'-dibromo-4,4'-dimethoxydiphenylamine (4):** A THF solution (180 mL) of **3** (26 g, 67 mmol) and *n*-tetrabutylammonium iodide (5.0 g, 13 mmol) was added dropwise to a stirred suspension of pulverized KOH in THF (90 mL) under an Ar atmosphere, and the reaction mixture was stirred for 1 h. A THF solution (90 mL) of benzyl bromide (9.0 mL, 76 mmol) was added dropwise to the stirred reaction mixture for 1 h, and then the resulting solution was heated at reflux overnight. The solvent was removed in vacuo. After addition of water and CH₂Cl₂, the organic layer was separated and dried over Na₂SO₄. After evaporation of the solvent, the crude product was purified by column chromatography on silica gel (CH₂Cl₂/*n*-hexane=1:1 as eluent) and was recrystallized from CH₃OH to afford **4** (23 g, 72%). ¹H NMR (400 MHz, CDCl₃): $\delta=7.50$ –

7.17 (m, 5H; CH₂Ph), 7.12 (d, ⁴*J*=3.0 Hz, 2H; H-3), 6.87 (d, ³*J*=9.0 Hz, 2H; H-6), 6.69 (dd, ³*J*=9.0, ⁴*J*=3.0 Hz, 2H; H-5), 4.67 (s, 2H; CH₂Ph), 3.60 ppm (s, 6H; OCH₃); ¹³C NMR (100 MHz, CDCl₃): $\delta=156.1$ (C_A-4), 140.5 (C_B-1), 138.1 (C_A-1), 128.1 (C_B-3), 127.7 (C_B-2), 126.9 (C_B-4), 125.5 (C_A-6), 121.9 (C_A-2), 119.3 (C_A-3), 113.5 (C_A-5), 57.3 (CH₂Ph or OCH₃), 55.6 ppm (CH₂Ph or OCH₃); elemental analysis calcd (%) for C₂₁H₁₉Br₂NO₂: C 52.86, H 4.01, Br 33.49, N 2.94; found: C 53.01, H 3.94, Br 33.56, N 2.86.

***N,N'*-Dibenzyl-10,10'-spirobi(2,8-dimethoxy-5,10-dihydrophenazasiline)**

(5): An *n*-hexane solution (1.65 M) of *n*BuLi (18.5 mL, 30.6 mmol) was added dropwise to a solution of **4** (7.3 g, 15.3 mmol) in Et₂O (300 mL) in an ice-cooled flask under an Ar atmosphere, and the reaction mixture was stirred for 20 min. SiCl₄ (0.88 mL) was added dropwise to the stirred reaction mixture. The resulting solution was stirred for 2 h, and then heated at reflux overnight. The solvent was removed in vacuo. After addition of water and CH₂Cl₂, the organic layer was separated and dried over Na₂SO₄. After evaporation of the solvent, the crude product was purified by column chromatography on silica gel (CH₂Cl₂ as eluent), and was washed with Et₂O to afford **5** as a white solid (3.0 g, 60%). ¹H NMR (400 MHz, CDCl₃): $\delta=7.43$ –7.29 (m, 10H; CH₂Ph), 6.95 (d, ³*J*=9.0 Hz, 4H; H-6), 6.89 (d, ⁴*J*=3.0 Hz, 4H; H-3), 6.83 (dd, ³*J*=9.0, ⁴*J*=3.0 Hz, 4H; H-5), 5.31 (s, 4H; CH₂Ph), 3.65 ppm (s, 12H; OCH₃); ¹³C NMR (100 MHz, CDCl₃): $\delta=153.0$ (C_A-4), 145.1 (C_B-1), 138.4 (C_A-1), 128.9 (C_B-3), 126.9 (C_B-2), 126.2 (C_B-4), 119.3 (C_A-6), 119.1 (C_A-2), 117.3 (C_A-3), 117.0 (C_A-5), 56.4 (CH₂Ph or OCH₃), 55.5 ppm (CH₂Ph or OCH₃); elemental analysis calcd (%) for C₄₂H₃₈N₂O₄Si: C 76.10, H 5.78, N 4.23; found: C 75.49, H 5.75, N 3.93.

10,10'-Spirobi(2,8-dimethoxy-5,10-dihydrophenazasiline) (6): A suspension of **5** (6.0 g, 9.1 mmol) and Pd on carbon (10%) in a mixed solvent of acetic acid and CH₂Cl₂ (180 mL) and CH₃OH (180 mL) was degassed repeatedly, and then vigorously stirred under H₂ gas overnight. The solvent was removed in vacuo, and then CH₂Cl₂ was added to the residue. After filtration through Celite, the solution was washed with alkaline water, and the organic layer was separated and dried over Na₂SO₄. After evaporation of the solvent, the crude product was purified by column chromatography on silica gel (CH₂Cl₂ as eluent), and was washed with Et₂O to afford **6** as a pale reddish powder (4.32 g, 99%). M.p. 265°C dec.; ¹H NMR (400 MHz, CDCl₃): $\delta=6.84$ (dd, ³*J*=9.0, ⁴*J*=3.0 Hz, 4H; H-5), 6.74 (d, ³*J*=9.0 Hz, 4H; H-6), 6.66 (d, ⁴*J*=3.0 Hz, 4H; H-3), 6.50 (br-s, 2H; NH), 3.54 ppm (s, 12H; OCH₃); ¹³C NMR (100 MHz, CDCl₃): $\delta=152.7$ (C-4), 141.4 (C-1), 119.2 (C_A-6), 118.6 (C_A-2), 116.1 (C_A-3), 114.3 (C_A-5), 55.6 ppm (OCH₃); elemental analysis calcd (%) for C₂₈H₂₆N₂O₄Si: C 69.69, H 5.43, N 5.80; found: C 69.28, H 5.45, N 5.64.

***N*-Anisyl-10,10'-spirobi(2,8-dimethoxy-5,10-dihydrophenazasiline) (7):** Anhydrous toluene (10 mL) was added to a mixture of **6** (229.4 mg, 0.48 mmol), *p*-bromoanisole (53 mL, 0.43 mmol), [Pd(dba)₂] (5.7 mg, 0.025 mmol), 2-(di-*tert*-butylphosphino)biphenyl¹³⁵ (15.0 mg, 0.050 mmol), and sodium *tert*-butoxide (81.0 mg, 0.88 mmol) in a flask under argon, and the solution was heated at reflux for 12 h. The solvent was removed in vacuo. After addition of water and CH₂Cl₂, the organic layer was separated and dried over Na₂SO₄. After evaporation of the solvent, the crude product was purified by column chromatography on silica gel (CH₂Cl₂/*n*-hexane=3:1 as eluent) to afford **7** as a pale yellow powder (136.6 mg, 54.0%). M.p. 155°C dec.; ¹H NMR (400 MHz, [D₆]acetone): $\delta=8.47$ (br-s, 1H; NH), 7.30 (m, 4H; H_C-2, H_C-3), 7.08 (d, ³*J*=9.0 Hz, 2H; H_A-6 or H_B-6), 6.96 (dd, ³*J*=9.0, ⁴*J*=2.9 Hz, 2H; H_A-5 or H_B-5), 6.79 (dd, ³*J*=9.3, ⁴*J*=3.2 Hz, 2H; H_A-5 or H_B-5), 6.78 (d, ⁴*J*=2.9 Hz, 2H; H_A-3 or H_B-3), 6.74 (d, ⁴*J*=3.2 Hz, 2H; H_A-3 or H_B-3), 6.48 (d, ³*J*=9.0 Hz, 2H; H_A-6 or H_B-6), 3.94 (s, 3H; Ar_C-OCH₃), 3.61 (s, 6H; Ar_A-OCH₃ or Ar_B-OCH₃), 3.56 ppm (s, 6H; Ar_A-OCH₃ or Ar_B-OCH₃); ¹³C NMR (100 MHz, [D₆]acetone): $\delta=160.0$ (C_C-4), 153.5, 153.4 (C_A-4, C_B-4), 145.8, 143.0 (C_A-1, C_C-1), 137.5 (C_C-1), 132.9 (C_B-2), 120.2, 119.3, 119.2, 118.8, 118.3 (C_A-2, C_A-3, C_B-3, C_B-6, C_C-2), 117.6, 117.5, 116.9, 114.1 (C_A-6, C_A-5, C_B-5, C_C-3), 55.9, 55.7, 55.5 ppm (Ar_A-OCH₃, Ar_B-OCH₃, Ar_C-OCH₃); FAB HRMS (*m*-nitrobenzyl alcohol): *m/z* (%): calcd for C₃₅H₃₂N₂O₅Si: 588.2080 [M]⁺; found 588.2080 (100).

Spirobi(trianisylamine) dimer (2): Anhydrous toluene (8 mL) was added to a mixture of **7** (220.0 mg, 0.37 mmol), *p*-dibromobenzene (29.4 mg,

0.12 mmol), [Pd(dba)₂] (3.6 mg, 0.0062 mmol), Ph₃FcP(*t*Bu)₂^[33,34] (8.9 mg, 0.012 mmol), and sodium *tert*-butoxide (23.0 mg, 0.25 mmol) in a flask under argon, and the solution was heated at reflux for 2 days. The solvent was removed in vacuo. After addition of water and CH₂Cl₂, the organic layer was separated and dried over Na₂SO₄. After evaporation of the solvent, the crude product was purified by column chromatography on silica gel (CH₂Cl₂/*n*-hexane = 5:2 as eluent) to afford **2** as a pale yellow powder (90.6 mg 58.1%). M.p. >300 °C; ¹H NMR (400 MHz, C₆D₆): δ = 7.46 (d, ⁴J = 3.0 Hz, 4H; H_{B-3} or H_{C-3}), 7.45 (d, ⁴J = 3.0 Hz, 4H; H_{B-3} or H_{C-3}), 7.40 (s, 4H; H_{A-2}), 7.18 (dd, ³J = 9.0, ⁴J = 2.2 Hz, 4H; H_{B-5} or H_{C-5}), 7.00 (d, ³J = 9.2 Hz, 4H; HD-3), 6.95 (dd, ³J = 9.3, ⁴J = 2.9 Hz, 4H; H_{B-5} or H_{C-5}), 6.86 (d, ³J = 8.6 Hz, 4H; H_{B-6} or H_{C-6}), 6.85 (d, ³J = 9.3 Hz, 4H; H_{B-6} or H_{C-6}), 6.77 (d, ³J = 9.2 Hz, 4H; HD-2), 3.34 (s, 6H; Ar_D-OCH₃), 3.18 (s, 12H; Ar_B-OCH₃ or Ar_C-OCH₃), 3.17 ppm (s, 12H; Ar_B-OCH₃ or Ar_C-OCH₃); ¹³C NMR (100 MHz, CDCl₃): δ = 158.9 (CD-4), 152.9, 152.4 (C_{B-4}, C_{C-4}), 145.2, 144.6 (C_{B-1}, C_{C-1}), 143.4, 136.7 (C_{A-1}, CD-1), 133.1, 132.2 (C_{B-2}, C_{C-2}), 119.9, 119.3, 118.5, 118.5 (C_{A-2}, C_{B-6}, C_{C-6}, CD-2), 118.1, 117.4, 117.2, 116.1 (C_{B-3}, C_{B-3}, C_{C-3}, C_{C-3}, CD-3), 55.6, 55.6, 55.6 ppm (Ar_B-OCH₃, Ar_C-OCH₃, Ar_D-OCH₃); FAB HRMS (*m*-nitrobenzyl alcohol): *m/z* (%): calcd for C₇₆H₆₆N₄O₁₀Si₂: 1250.4317 [M]⁺; found 1250.4327 (9.9).

X-ray crystallographic analysis: A single crystal of **2** for X-ray studies was obtained as 2·(CH₃CN)₄·(H₂O) from acetonitrile/CH₂Cl₂ by slow evaporation. Data collections were performed on a Rigaku RAXIS RAPID imaging plate area detector with graphite-monochromated Cu_{Kα} radiation at 93 K. The data were corrected for Lorentz and polarization effects. The structure was solved using direct methods (SHELXL-97),^[48] expanded by using Fourier techniques (DIRDIF-99),^[49] and refined by full-matrix least-squares of *F*² on the basis of 6478 observed reflections and 486 variable parameters (SHELXL-97).^[48] The non-hydrogen atoms were refined anisotropically. Hydrogen atoms were refined by using the riding model. All the calculations were performed by using CrystalStructure crystallographic software package,^[50] except for refinement. CCDC-781527 contains the supplementary crystallographic data for this paper. These data can be obtained free of charge from The Cambridge Crystallographic Data Centre via www.ccdc.cam.ac.uk/data_request/cif.

Acknowledgements

This work was supported by a Grant-in-Aid for Scientific Research (B) (20350065) from the Japan Society for the Promotion of Science (JSPS). Thanks are due to the Instrument Center, the Institute for Molecular Science, for the use of a pulsed ESR spectrometer.

- C. Joachim, J. K. Gimzewski, A. Aviram, *Nature* **2000**, *408*, 541–548.
- R. L. Carroll, C. B. Gorman, *Angew. Chem.* **2002**, *114*, 4556–4579; *Angew. Chem. Int. Ed.* **2002**, *41*, 4378–4400.
- A. Nitzan, M. A. Ratner, *Science* **2003**, *300*, 1384–1389.
- L. McElwee-White, W. A. Goddard III, D. A. Dougherty, *J. Am. Chem. Soc.* **1984**, *106*, 3461–3466.
- L. McElwee-White, D. A. Dougherty, *J. Am. Chem. Soc.* **1984**, *106*, 3466–3474.
- A. Farazdel, M. Dupuis, E. Clementi, A. Aviram, *J. Am. Chem. Soc.* **1990**, *112*, 4206–4214.
- P. Maslak, M. P. Augustine, J. D. Burkey, *J. Am. Chem. Soc.* **1990**, *112*, 5359–5360.
- K. Ueda, M. Yamano, T. Sugimoto, H. Fujita, A. Ugawa, K. Yakushi, K. Kano, *Chem. Lett.* **1997**, 461–462.
- X. Chi, M. E. Itkis, B. O. Patrick, T. M. Barclay, R. W. Reed, R. T. Oakley, A. W. Cordes, R. C. Haddon, *J. Am. Chem. Soc.* **1999**, *121*, 10395–10402.
- M. E. Itkis, X. Chi, A. W. Cordes, R. C. Haddon, *Science* **2002**, *296*, 1443–1445.
- S. K. Pal, M. E. Itkis, F. S. Tham, R. W. Reed, R. T. Oakley, R. C. Haddon, *Science* **2005**, *309*, 281–284.
- R. C. Haddon, A. Sarkar, S. K. Pal, X. Chi, M. E. Itkis, F. S. Tham, *J. Am. Chem. Soc.* **2008**, *130*, 13683–13690.
- W. Setaka, C. Kabuto, M. Kira, *Chem. Lett.* **1999**, 317–318.
- N. L. Frank, R. Clérac, J.-P. Sutter, N. Daro, O. Kahn, C. Coulon, M. T. Green, S. Golhen, L. Ouahab, *J. Am. Chem. Soc.* **2000**, *122*, 2053–2061.
- T. Ishida, M. Ooishi, N. Ishii, H. Mori, T. Nogami, *Polyhedron* **2007**, *26*, 1793–1799.
- H. Dürr, R. Gleiter, *Angew. Chem.* **1978**, *90*, 591–601; *Angew. Chem. Int. Ed. Engl.* **1978**, *17*, 559–569.
- A. Ito, M. Urabe, K. Tanaka, *Angew. Chem.* **2003**, *115*, 951–954; *Angew. Chem. Int. Ed.* **2003**, *42*, 921–924, see also correction: *Angew. Chem. Int. Ed.* **2009**, *48*, 5785.
- Y. Hirao, M. Urabe, A. Ito, K. Tanaka, *Angew. Chem.* **2007**, *119*, 3364–3367; *Angew. Chem. Int. Ed.* **2007**, *46*, 3300–3303.
- M. C. Böhm, R. Gleiter, *J. Chem. Soc. Perkin Trans. 2* **1979**, 443–448.
- K. Okada, T. Imakura, M. Oda, H. Murai, M. Baumgarten, *J. Am. Chem. Soc.* **1996**, *118*, 3047–3048.
- V. M. Domingo, C. Alemán, E. Brillas, L. Juliá, *J. Org. Chem.* **2001**, *66*, 4058–4061.
- E. Terada, T. Okamoto, M. Kozaki, M. E. Masaki, D. Shiomi, K. Sato, T. Takui, K. Okada, *J. Org. Chem.* **2005**, *70*, 10073–10081.
- M. Baumgarten, U. Müller, A. Bohnen, K. Müllen, *Angew. Chem.* **1992**, *104*, 482–485; *Angew. Chem. Int. Ed. Engl.* **1992**, *31*, 448–451.
- M. Baumgarten, W. Huber, K. Müllen, *Adv. Phys. Org. Chem.* **1993**, *28*, 1–44.
- U. Müller, M. Baumgarten, *J. Am. Chem. Soc.* **1995**, *117*, 5840–5850.
- Gaussian 03, Revision D.02, M. J. Frisch, G. W. Trucks, H. B. Schlegel, G. E. Scuseria, M. A. Robb, J. R. Cheeseman, J. A. Montgomery, Jr., T. Vreven, K. N. Kudin, J. C. Burant, J. M. Millam, S. S. Iyengar, J. Tomasi, V. Barone, B. Mennucci, M. Cossi, G. Scalmani, N. Rega, G. A. Petersson, H. Nakatsuji, M. Hada, M. Ehara, K. Toyota, R. Fukuda, J. Hasegawa, M. Ishida, T. Nakajima, Y. Honda, O. Kitao, H. Nakai, M. Klene, X. Li, J. E. Knox, H. P. Hratchian, J. B. Cross, V. Bakken, C. Adamo, J. Jaramillo, R. Gomperts, R. E. Stratmann, O. Yazyev, A. J. Austin, R. Cammi, C. Pomelli, J. W. Ochterski, P. Y. Ayala, K. Morokuma, G. A. Voth, P. Salvador, J. J. Dannenberg, V. G. Zakrzewski, S. Dapprich, A. D. Daniels, M. C. Strain, O. Farkas, D. K. Malick, A. D. Rabuck, K. Raghavachari, J. B. Foresman, J. V. Ortiz, Q. Cui, A. G. Baboul, S. Clifford, J. Cioslowski, B. B. Stefanov, G. Liu, A. Liashenko, P. Piskorz, I. Komaromi, R. L. Martin, D. J. Fox, T. Keith, M. A. Al-Laham, C. Y. Peng, A. Nanayakkara, M. Challacombe, P. M. W. Gill, B. Johnson, W. Chen, M. W. Wong, C. Gonzalez, J. A. Pople, Gaussian, Inc., Wallingford CT, **2004**.
- B. O. Roos, *Adv. Chem. Phys.* **1987**, *69*, 399–446.
- D. Wittenberg, H. A. McNince, H. Gilman, *J. Am. Chem. Soc.* **1958**, *80*, 5418–5422.
- J. P. Wolfe, S. Wagaw, J. F. Marcoux, S. L. Buchwald, *Acc. Chem. Res.* **1998**, *31*, 805–818.
- J. F. Hartwig, *Acc. Chem. Res.* **1998**, *31*, 852–860.
- J. F. Hartwig, *Angew. Chem.* **1998**, *110*, 2154–2177; *Angew. Chem. Int. Ed.* **1998**, *37*, 2046–2067.
- A. R. Muci, S. L. Buchwald, *Top. Curr. Chem.* **2002**, *219*, 131–209.
- Q. Shelby, N. Kataoka, G. Mann, J. F. Hartwig, *J. Am. Chem. Soc.* **2000**, *122*, 10718–10719.
- N. Kataoka, Q. Shelby, J. P. Stambuli, J. F. Hartwig, *J. Org. Chem.* **2002**, *67*, 5553–5566.
- J. P. Wolfe, H. Tomori, J. P. Sadighi, S. L. Buchwald, *J. Org. Chem.* **2000**, *65*, 1158–1174.
- D. M. D'Alessandro, F. R. Keene, *Dalton Trans.* **2004**, 3950–3954.
- F. Barrière, N. Camire, W. E. Geiger, U. T. Mueller-Westerhoff, R. Sanders, *J. Am. Chem. Soc.* **2002**, *124*, 7262–7263.
- F. Barrière, W. E. Geiger, *J. Am. Chem. Soc.* **2006**, *128*, 3980–3989.
- S. Santì, L. Orian, C. Durante, E. Z. Bencze, A. Bisello, A. Donoli, A. Cecon, F. Benetollo, L. Crociani, *Chem. Eur. J.* **2007**, *13*, 7933–7947.

- [40] F. A. Bell, A. Ledwith, D. C. Sherrington, *J. Chem. Soc.* **1969**, 2719–2720.
- [41] W. Weltner, Jr., *Magnetic Atoms and Molecules*, Dover, New York, **1989**.
- [42] J. Isoya, H. Kanda, J. R. Norris, J. Tang, M. K. Brown, *Phys. Rev. B* **1990**, *41*, 3905–3913.
- [43] A. V. Astashkin, A. Schweiger, *Chem. Phys. Lett.* **1990**, *174*, 595–602.
- [44] K. Sato, M. Yano, M. Furuichi, D. Shiomi, T. Takui, K. Abe, K. Itoh, A. Higuchi, K. Katsuma, Y. Shirota, *J. Am. Chem. Soc.* **1997**, *119*, 6607–6613.
- [45] Y. Hirao, H. Ino, A. Ito, K. Tanaka, T. Kato, *J. Phys. Chem. A* **2006**, *110*, 4866–4872.
- [46] Elemental analysis calcd for $C_{76}H_{66}N_4O_{10}Si_2Sb_4Cl_{24} [2^{4+}(SbCl_6)_4]$: C 35.25, H 2.57, N 2.16, Cl 32.86; found: C 35.12, H 2.58, N 2.17, Cl 31.12.
- [47] E. Sinn, *Coord. Chem. Rev.* **1970**, *5*, 313–347.
- [48] Program for Crystal Structure Solution and Refinement, G. M. Sheldrick, Universität Göttingen, **1997**.
- [49] The DIRDIF-99 Program System, Technical Report of the Crystallography Laboratory, P. T. Beurskens, G. Admiraal, G. Beurskens, W. P. Bosman, R. de Gelder, R. Israel J. J. M. Smits, University of Nijmegen (The Netherlands), **1999**.
- [50] CrystalStructure 3.8, Crystal Structure Analysis Package; Rigaku and Rigaku/MSC, Woodlands, **2000–2006**.

Received: April 5, 2010

Revised: June 18, 2010

Published online: July 30, 2010